NUMERICAL SIMULATION OF FRACTURE IN CONCRETE USING JOINT ELEMENTS

V. O. García-Álvarez, I .Carol and R .Gettu.

E.T.S. de Ingenieros de Caminos, Canales y Puertos
Universitat Politècnica de Catalunya
Campus Nord, Gran Capità s/n, 08034 Barcelona
España

Resumen. En este artículo se recogen los resultados preliminares obtenidos en el desarrollo de un modelo numérico para analizar el comportamiento de los materiales cuasifrágiles y simular la formación de fisuras. Para ello se utiliza el Método de los Elementos Finitos con elementos junta en el plano esperado de fisura. La ley de comportamiento de estos elementos corresponde a una ley de fisura cohesiva con G_f predeterminada. La resolución del problema de contorno exige la utilización de estrategias numéricas avanzadas tipo "arc-length" o IDC.

Abstract. In this paper, the preliminary results obtained in the development of a numerical model for fracture of quasi-brittle materials are presented and discussed. The model is based on the FEM with joint elements along the expected crack path. Material laws of the joints correspond to a cohesive crack model with given G_f. Advanced solution techniques such as the arc-length or IDC are needed due to the possibility of snap-back in the resulting force-displacement diagram.

1. INTRODUCTION.

The main objective of ongoing studies, from which some preliminary results are presented here, is the modeling of cracking and fracture problems in Mode I (tensile), and under mixed mode conditions (shear tension and shear compression).

For this purpose a nonlinear finite element code has been developed where cracks can be modeled with joint elements. A nonlinear cohesive-crack constitutive law has been implemented and is being used to solve typical examples of fracture in quasi-brittle materials such as concrete.

It is well known that in Mode I and Mixed Mode fracture experiments the load-displacement relation may exhibit snap-back. Classical finite element analysis techniques only control the load or displacement at selected nodes. This type of control is inadequate for the solution of problems with snap-back. To overcome this, advance solution strategies such as the arc-length and IDC techniques have been incorporated in the code.

In this paper, some results obtained for Mode I tensile and bending experiments, are presented.

2. DISCRETE CRACK MODELS.

The basic theory for structural analysis is Continuum Mechanics (CM). The equations given by this theory are valid for continuum media. However, a crack is a discontinuity in the solid, and, therefore, the use of CM requires some extra assumptions with limited validity. The adaptation of CM to a cracked media has traditionally originated two large families of models known as the smeared crack (SC) models and the discrete crack (DC) models. However, after a clearly differentiated beginning, their precise definition and the differences between them are matter of increasing debate in the literature [1–13].

The approach followed in this work proceeds in the line suggested in recently years by other authors

[4–5,9,12]. It can be mainly considered as a DC model, although it incorporates joint elements that were not used in the classical implementation of that approach. Three of the main difficulties of classical DC models are: *(i)* in a classical finite element analysis these models imply a continuous change in the mesh; *(ii)* the crack must pass through a prescribed path between the finite elements, which causes a directional bias in the final solution; and, *(iii)* it is difficult to study at the same time the evolution of several (i.e., more than two or three) cracks in a body. The first two of the aforementioned drawbacks have been more or less overcome with the use of the joint elements and mesh generators. The third one has limited in practice the use of the discrete crack models to cases of localized fracture, such as the case of Mode I fracture beams.

3. JOINT ELEMENT.

The main characteristic of the joint elements employed is that geometrically they are of the "zero thickness" type (thickness can be set to a certain small value or simply to zero with no additional difficulties).

Due to the necessary compatibility with the continuum elements on both sides, the geometry, the number of nodes and other aspects of the joint element are given. In this case, eight-node quadrilateral and six-node triangular quadratic elements are considered, and therefore, the corresponding joint element is the one represented in Fig. 1.

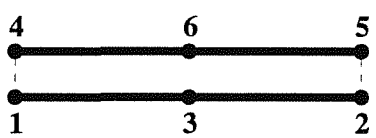

Fig. 1. Quadratic joint element.

The choice of the integration rule for the joint element is a crucial point since standard Gauss can lead to " bumpy" results with spurious jumps in the stress and strain fields [14–15]. Here, the solution first proposed in [14] is followed. The integration rule used is the Simpson-Lobatto scheme with three points (equivalent to the closing Newton-Cotes rule of integration with three points; see [14–15]).

4. COHESIVE CRACK LAW.

The constitutive law used for the joints elements is linear elasticity in shear and that of a Dugdale-type cohesive crack in tension. Since the use of cohesive crack models [16], this family of constitutive laws are the most popular in the discrete crack modeling with nonlinear material behavior. A more sophisticated coupled shear-normal cohesive crack law is now under development for future applications when shear in the crack plane can be of importance [7]. The normal law is represented in Fig. 2.

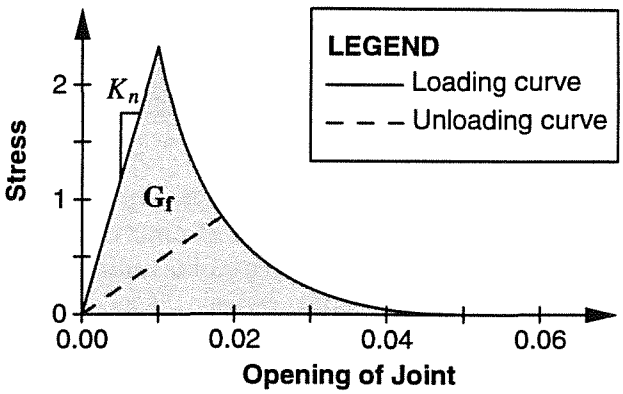

Fig. 2. Exponential cohesive crack law.

The descending branch of the diagram is given by the following equation:

$$\sigma = f_t \exp\left(\frac{u - u_p}{c}\right) \qquad (1)$$

where

$$u_p = \frac{f_t}{K_n} \quad \text{and} \quad c = \frac{G_c}{f_t} - \frac{f_t}{2\,K_n} \qquad (2, 3)$$

with

f_t: Tensile strength.
K_n: Normal stiffness.
G_c: Fracture energy.
u_p: The opening at which $\sigma = f_t$.

In compression, the law follows the elastic behavior

$$\sigma = u_p\, K_n \qquad (4)$$

A secant stiffness is assumed for unloading-reloading under tension.

The assumption of a constant elastic stiffness in compression is not in full agreement with the results of normal tests on joints, which suggest a "locking" behavior with a limit value of the relative displacement in closing. High values of K_n can, however, limit in practice the closure values, and avoid the unpleasant and complex mixed initial-stress/initial-strain implementations of the constitutive law which are necessary to cope with such a closure limit [14,17].

5. FINITE ELEMENT ANALYSIS WITH ADVANCED ITERATIVE STRATEGIES.

Standard FE formulations are based on the three following equations for equilibrium, material behavior and strain-displacement laws:

$$\int_{\bar{\Omega}} \mathbf{B}^{\mathrm{T}} \boldsymbol{\sigma}\, d\Omega = \mathbf{F} \tag{5a}$$

$$\boldsymbol{\sigma} = \boldsymbol{\sigma}(\text{history of } \boldsymbol{\epsilon}) \tag{5b}$$

$$\boldsymbol{\epsilon} = \mathbf{B}\mathbf{a} \tag{5c}$$

where:

- **a**: vector of nodal displacements
- **B**: gradient matrix
- $\boldsymbol{\sigma}$: stress vector
- $\bar{\Omega}$: domain of the body
- **F**: vector of nodal forces

These equations can be solved for prescribed values of the components of **F** or **a** for every degree of freedom, if no snap-back occurs in the **F**–**a** curve. In cases with snap-back, the values of **F** or **a** cannot be prescribed in advance, and the arc-length or some Indirect Displacement Control (IDC) method must be incorporated [18–21]. For that, one must rewrite Eqn. (5a) for a given (real or fictitious) time increment (K), as

$$\int_{\bar{\Omega}} \mathbf{B}^{\mathrm{T}} \Delta\boldsymbol{\sigma}^{(K)} d\Omega = \Delta\lambda^{(K)}\, \mathbf{f} \tag{6}$$

where $\Delta\boldsymbol{\sigma}^{(K)}$ represents the increment of stresses, **f** is a known vector of nominal loads and $\Delta\lambda^{(K)}$ is the loading factor, an additional unknown to solve with **a** throughout calculation. This necessitates an additional constraint equation of the type

$$\Delta\ell^{(K)} = \Delta\ell(\Delta\mathbf{a}^{(K)}, \Delta\lambda^{(K)}) \tag{7}$$

where $\Delta\ell^{(K)}$ is prescribed. Eqn. (7) states the actual condition for determining the "size" of the increment as a function of the increment of nodal displacements and (sometimes) $\Delta\lambda^{(K)}$. Various definitions of Eqn. (7) lead to different arc-length or IDC procedures [18–21]. In this case, the following expression has been used:

$$\Delta\ell^{(K)2} = \Delta\bar{\mathbf{a}}^{T} \Delta\bar{\mathbf{a}} \tag{8}$$

where $\bar{\mathbf{a}}$ is a vector with reduced number of components that are linear combinations with fixed coefficients of the nodal displacements

$$\bar{\mathbf{a}} = \mathbf{C}\mathbf{a} \tag{9}$$

Note that this definition includes as particular cases the classical arc-length procedure when $\mathbf{C} = \mathbf{I}$ and $\bar{\mathbf{a}} = \mathbf{a}$, and also a variety of IDC procedures (such as CMOD control, etc.) when $\bar{a}$ includes a reduced number of relative displacements between selected points on the specimen.

The numerical implementation of this method requires to solve Eqn. (6) by Newton-Raphson-type procedures leading to

$$\mathbf{K_j} \Delta\Delta\mathbf{a}_j^{(K)} = \mathbf{R}_{j-1} + \Delta\Delta\lambda_j^{(K)} \mathbf{f} \tag{10}$$

where $\Delta\Delta\mathbf{a}_j^{(K)}$ and $\Delta\Delta\lambda_j^{(K)}$ denote the increments of $\Delta\mathbf{a}^{(K)}$ and $\Delta\lambda^{(K)}$ in the jth iteration, and $\mathbf{R}_{j-1}$ is the residual from the previous iteration $j-1$

$$\mathbf{R}_{j-1} = \Delta\lambda_{j-1}^{(K)} \mathbf{f} - \int_{\bar{\Omega}} \mathbf{B}^{\mathrm{T}} \Delta\boldsymbol{\sigma}_{j-1}^{(K-1)} d\Omega \tag{11}$$

The second term on the right-hand side of Eqn. (10) is the increment of forces due to change of the loading factor λ. From Eqn. (10) one obtains

$$\Delta\Delta\mathbf{a}_j^{(K)} = \mathbf{b}^{I} + \Delta\Delta\lambda_j^{(K)} \mathbf{b}^{II} \tag{12}$$

where $\mathbf{b}^{I}$ and $\mathbf{b}^{II}$ are vectors known at the beginning of the calculation of the jth iteration as

$$\mathbf{b}^{I} = \mathbf{K_j}^{-1} \mathbf{R}_{j-1} \quad ; \quad \mathbf{b}^{II} = \mathbf{K_j}^{-1} \mathbf{f} \tag{13}$$

Introducing Eqns. (12) and (9) into the constraint (8), one obtains the following equation quadratic in $\Delta\Delta\lambda_j^{(K)}$:

$$C_1 \left(\Delta\Delta\lambda_j^{(K)}\right)^2 + C_2\, \Delta\Delta\lambda_j^{(K)} + C_3 = 0 \tag{14a}$$

with:

$$C_1 = \mathbf{b}^{II\,T} \mathbf{C}^{\mathrm{T}} \mathbf{C}\, \mathbf{b}^{II} \tag{14b}$$

$$C_2 = 2(\mathbf{b}^{II\,T} \mathbf{C}^{\mathrm{T}} \mathbf{C}\, \mathbf{b}^{I}) \tag{14c}$$

$$C_3 = \mathbf{b}^{I\,T} \mathbf{C}^{\mathrm{T}} \mathbf{C}\, \mathbf{b}^{I} - \Delta\ell_j^{(K)2} \tag{14d}$$

By choosing the appropriate root of Eqn. (14), the increment of the load factor in the jth iteration can be finally obtained.

In IDC procedures, Eqn. (14) needs to be solved in fact only for the first iteration. For further iterations, one can use the linearized form obtained through differentiation of Eqn. (8)

$$\Delta\bar{\mathbf{a}}_{j-1}^{T} \Delta\Delta\bar{\mathbf{a}}_j = 0 \tag{15}$$

By replacing Eqns. (9) and (12) in this equation, one obtains after some rearrangement the expression of the loading factor:

$$\Delta\Delta\lambda_j^{(K)} = -\frac{\Delta\mathbf{a}_{j-1}^{(K)\,T}\mathbf{C}^{\mathrm{T}}\mathbf{C}\,\mathbf{b}^{I}}{\Delta\mathbf{a}_{j-1}^{(K)\,T}\mathbf{C}^{\mathrm{T}}\mathbf{C}\,\mathbf{b}^{II}} \qquad (16)$$

6. EXAMPLES.

The first example represents a joint element embedded between two continuum elements of dimensions 1×1, which are loaded in pure tension (Fig. 3).

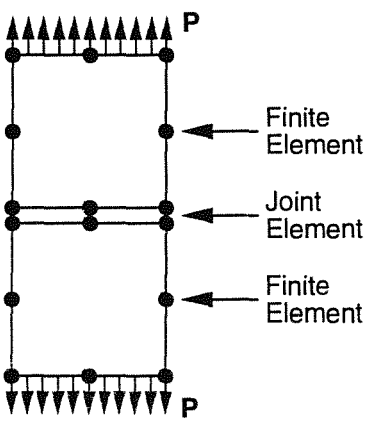

Fig. 3. First example.

The main objective of this example is the verification of the numerical techniques employed. The parameters used are $E = 10^5$ (continuum elements), $K_n = K_t = 10^5$ (normal and shear stiffness of the joint), $f_t = 100$ (maximum tensile stress of the joint).

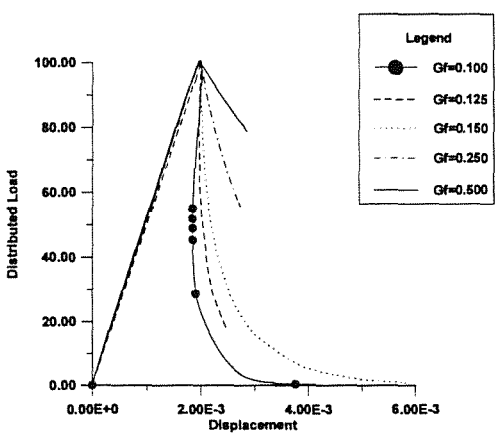

Fig. 4. Results of the first example run with the arc-length method.

Various calculations were performed with different (decreasing) values of G_f, starting with $G_f = 0.500$. For this value, the results obtained did not show snap-back, but for lower values, the snap-back becomes apparent. G_f has also a minimum value of 0.05 since for that value the initial slope after the peak at the constitutive law for the joint (Fig. 2) becomes vertical, which makes calculations impossible. This example was run using both arc-length (Fig. 4) and IDC (opening of the joint) methods (Fig. 5).

Convergence problems were encountered with the arc-length method for G_f lower than 0.100, and due to this no results are plotted in Fig. 4. In contrast, the IDC method performs well up to $G_f = 0.051$, which seem to confirm that this technique is more suitable for material nonlinearities with high degrees of localization, as already suggested in [21].

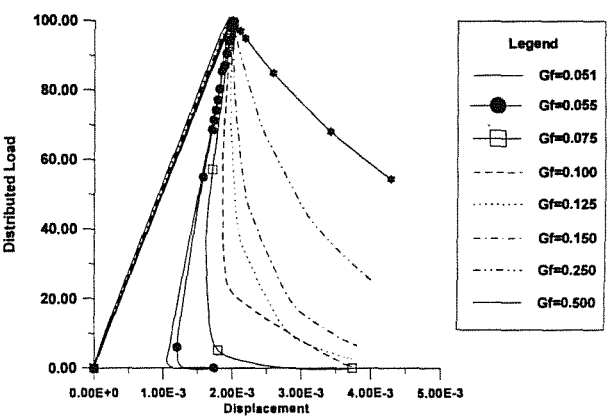

Fig. 5. Results of the first example run with IDC.

The second example is a three-point bent beam of dimensions $a = 0.25d$ and $d = 100$ mm [22] (Fig. 6).

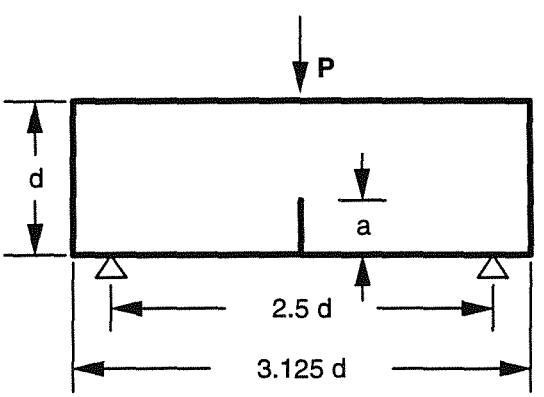

Fig. 6. Second example.

The mesh used in the finite element analysis can be seen in Fig. 7. The stresses obtained along the joints using two different integration rules are plotted and compared with stresses obtained without using joint elements.

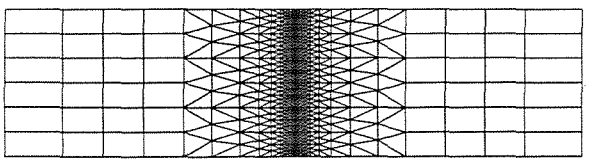

Fig. 7. Mesh of the second example.

Fig. 8 shows that the joint element gives the same stresses in the elastic stage as calculated without joint elements, except at the two ends of the ligament. This difference is caused by the effects of the concentrated load and of the crack tip. The results also exhibit the jumps in stresses that can be obtained with joint elements if an inappropriate integration scheme is used (in this case, Gauss, see [14,15]).

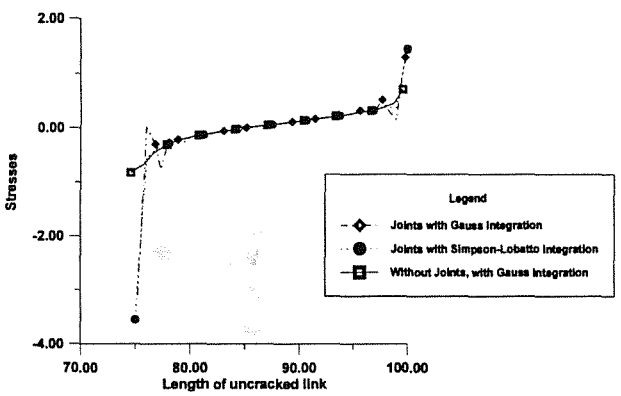

Fig. 8. Stress along the uncracked link of a beam using LEFM.

Fig. 9 depicts the results of the second example using the cohesive crack law of Fig. 2. The parameters of this example are $E = 20000$ MPa, $K_n = K_t = 10^6$ N/mm (normal and shear stiffness of the joint), $f_t = 2.4$ MPa (maximum tensile stress of the joint). The figure shows a standard force-displacement diagram for high values of G_f, which shrinks and evolves into a sharper peak and snap-back for lower values of G_f. Work is still under way to investigate effects of the other parameters such as E, the dimensions of the beam, etc.

7. CONCLUSIONS.

A numerical model for the fracture of quasi-brittle materials has been presented. The use of joint elements to simulate discrete cracking has several advantages and is easy to implement in existing numerical codes. Arc-length or IDC techniques are necessary in the presence of snap-back in the force displacement diagram. The latter method with CMOD control seems to perform better in problems with highly localized phenomena such as cracking. Lower G_f values lead to sharper peaks and eventually to snap-back in the load-displacement curves, as demonstrated for three-point bent tests.

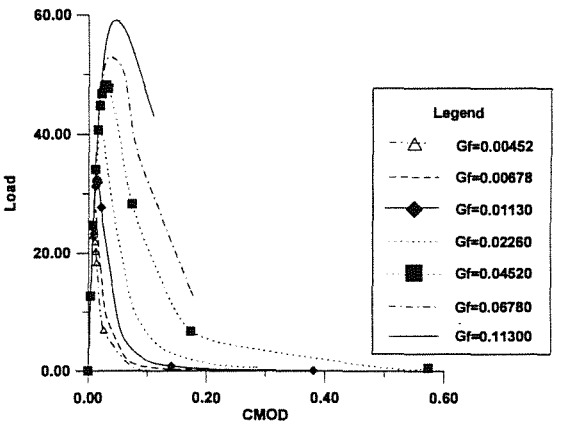

Fig. 9. Results of the second example using a Cohesive Crack Law and IDC.

8. ACKNOWLEDGEMENTS

Partial support from the DGICYT (Madrid, Spain) under research projects PB90-0598 and PB92-0702 is greatly appreciated. The first author is grateful for a fellowship from the Comissionat per a Universitats i Recerca of the Generalitat de Catalunya (Barcelona, Spain). The authors thank Prof. P.C. Prat from our Department, for his valuable assistance with the computer-related work and for the stimulating technical discussions.

9. REFERENCES

[1] Ngo, D. and Scordelis, A., "Finite element analysis of reinforced concrete beams," ACI Journal **64-14**, 152–163 (1967).

[2] Rashid, Y. R., "Ultimate strength analysis of prestressed concrete pressure vessels," Nuclear Engineering and Design, **7**, 334–344 (1968).

[3] Ingraffea, A. R., "Non–linear fracture models for discrete crack propagation," Application of Fracture Mechanics to Cementitious Composites, ed. S. P. Shah, 171–209 (1984).

[4] Rots, J. G., "Computational Modeling of Concrete Fracture," Ph.D. Thesis (1988).

[5] Rots, J. G. and Blaauwendrad, J., "Crack models for concrete: Discrete or Smeared? Fixed, multi-directional or rotating?," Heron, **34** (1989).

[6] Carol, I. and Prat, P. C., "Smeared analysis of concrete fracture using a microplane based multi-crack model with static constraint," Fracture Processes in Concrete, Rock and Ceramics, ed. J. G. M. van Mier (1991).

[7] Carol, I., Prat P. C., and Gettu, R., "Numerical analysis of mixed-mode fracture of quasi–brittle materials using a multicrack constitutive model," Mixed-Mode Fatigue and Fracture, Rossmanith and Miller (eds.), 319–331 (1991).

[8] Lofti, H. R. and Shing, P. B., "An appraisal of smeared crack models for masonry shear wall analysis," Computers and Structures, **41**, 413–425 (1991).

[9] Gerstle, W. H. and Xie, M., "FEM modeling of fictitious crack propagation in concrete," Journal of Engineering Mechanics, **118**, 416–434 (1992).

[10] Lofti, H. R., "Finite element analysis of fracture of concrete and masonry structures," Ph. D. Thesis (1992).

[11] Oliver, J., "Smeared crack models: fundamentals and applications," Notes for the Comett Course on Fracture Mechanics of Concrete (1992).

[12] Schellekens, J. C. J., "Computational strategies for composite structures," Ph. D. Thesis (1992).

[13] Lofti, H. R., "Finite element analysis of fracture of concrete and masonry structures," Journal of Structural Engineering, **120**, 63–80 (1994).

[14] Gens, A., Carol, I. and Alonso, E. E., "An interface element formulation for the analysis of soil-reinforcement interaction," Computers and Geotechnics, **7**, 133–151 (1988).

[15] Schellekens, J. C. J., "Interface elements in finite element analysis," TU-Delft, Report 25-2-90-5-17 (1990).

[16] Hillerborg, A., Mordeer, M. and Petersson, P.-E., "Analysis of crack formation and crack growth in concrete by means of fracture mechanics and finite elements," Cement and Concrete Research, **6**, 773–782 (1976).

[17] Gens, A., Carol, I. and Alonso, E. E., "Elasto-plastic model for joints and interfaces," Computational Plasticity, ed. E. Oñate et al., 1251–1264 (1989).

[18] Riks, E., "The application of Newton's method to the problem of elastic stability," Journal of Applied Mechanics, **39**, 1060–1066 (1972).

[19] Crisfield, M. A., "Accelerated solutions techniques and concrete cracking," Computer Methods in Applied Mechanics and Engineering **33**, 585–607 (1981).

[20] de Borst, R. (1987), "Computation of post-bifurcation and post-failure behavior of strain softening solids," Computers & Structures, **25**, 211–224.

[21] Foster, S., "An application of the arc-length method involving concrete cracking," International Journal for Numerical Methods in Engineering, **33**, 269–285 (1992).

[22] Karihaloo, B. L. and Nallathambi, P., "Notched beam test: Mode I fracture toughness," Fracture Mechanics Test Methods for Concrete, ed. S. P. Shah and A. Carpinteri, 1–86 (1991).